BATCH-FABRICATED MEMS RETARDING POTENTIAL ANALYZER FOR HIGH-ACCURACY ION ENERGY MEASUREMENTS

E. V. Heubel[*] *and L. F. Velásquez-García*
Massachusetts Institute of Technology, Cambridge, Massachusetts, USA

ABSTRACT

We report the design, fabrication, and experimental characterization of a novel fully microfabricated retarding potential analyzer (RPA) with performance better than the state-of-the-art. Our device comprises a set of bulk-micromachined electrode grids with apertures and inter-electrode spacing compatible with high-density plasma measurements; the thick electrodes also make our ion energy sensor more resistant to ablation in harsh environments than previously reported miniaturized RPAs. Our RPA includes a set of microfabricated deflection springs for robust and compliant alignment of the grid apertures across the grid stack, which greatly increases the signal strength and minimizes the ion interception, resulting in a tenfold improvement in peak signal amplitude compared to an RPA with unaligned grids and similar inter-electrode spacing.

INTRODUCTION

Plasmas, i.e., quasi-neutral ionized gases, enable a broad range of exciting technological applications. For example, plasma fusion reactors, e.g., tokamaks, are currently investigated as an attractive approach to generate great amounts of green energy at a very low cost. Also, plasma thrusters have been developed to accomplish in-space missions while consuming a fraction of the propellant that a chemical rocket would spend. In addition, plasma sources are used for processing Complementary Metal Oxide Semiconductor (CMOS) devices, from ion implantation to thin film deposition to etching, due to their great controllability and repeatability, as well as their unmatched capability to define very small features in parallel. Moreover, plasma sources are used in mass spectrometry to ionize the analyte prior to electromagnetic filtering. In each of these applications, characterization of the properties of the plasma greatly increases the controllability of the process they harness. An important plasma property in the aforementioned applications is the ion energy, as it relates to the velocity with which ions collide with surfaces; a flux of energetic ions can etch, dope, or ablate material from a surface, and it can also affect surface reaction rates.

A retarding potential analyzer (RPA) can be used to directly measure the ion energy distribution. A typical RPA is composed of four perforated electrodes, i.e., grids, and a solid electrode, i.e., a collector, that are biased at various voltages to accomplish energy-based ion filtering. As shown in Figure 1: the floating grid establishes a floating potential, V_f, that traps the plasma outside the sensor; the first electron-repelling grid, biased at a negative voltage V_{e-}, removes the electrons from the particle beam; the ion-retarding grid, biased at a variable potential V_{ion}, progressively shields more energetic ions as it is swept from a low potential to a high potential; the ion current is intercepted by the innermost electrode, i.e., the collector, after passing through a second electron-repelling grid that prevents secondary electron emission from the collector. The collector current is representative of the cumulative ion energy distribution; assuming that all ions are singly ionized, the derivative of this signal with respect to the ion retarding voltage is directly proportional to the energy distribution [1].

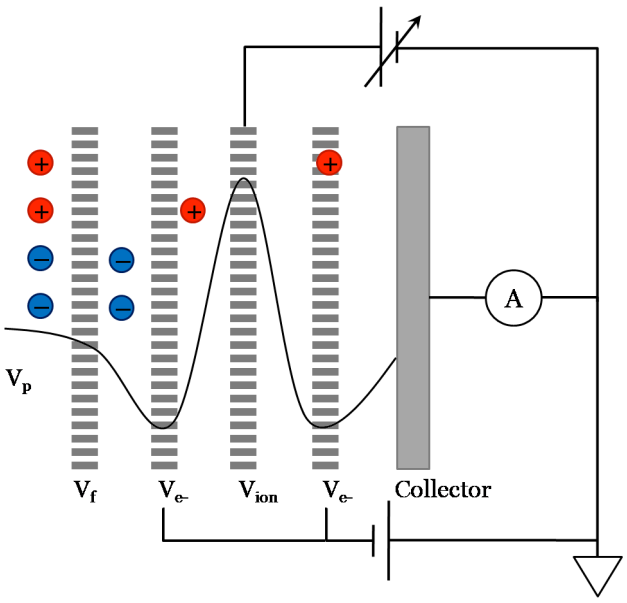

Figure 1: RPA schematic to measure the ion energy of a plasma at V_p potential.

Numerous RPAs have been reported; most of them vary the number of grids, materials chosen, aperture sizes, or introduce collimators [2]-[6]. However, conventional means of fabrication have limited the use of RPAs with plasmas of small Debye lengths – related to plasmas with high density and/or low energy. RPAs with grids made of woven stainless steel, molybdenum wire mesh, photo-chemically, and laser etched grids have small electrode stack transparency due to the inherent difficulties of aligning thin meshes that are prone to warpage; additionally, with these materials, inter-grid spacing of 0.5mm or less is difficult to maintain [7], which limits the minimum Debye length compatible with the device. Single-orifice RPAs have been reported [8],[9] to allow sensing of plasmas with small Debye lengths; this design uses two ion-retarding electrodes held at the same bias voltage to avoid electric field cupping; however, these devices have very small output signal strength as the grids have a single aperture. By utilizing microelectromechanical systems (MEMS) fabrication methods, we were able to implement RPAs with the required micron scale features for small-Debye length plasmas without affecting the output signal strength of the sensor. This work builds on previous results presented at Hilton Head 2012 [10].

DESIGN

Figure 2 shows a schematic of our MEMS RPA, where curved silicon springs are utilized to fasten and reference a set of grids to achieve proper stack alignment; the gap between successive electrodes is simply defined by the difference in thickness between the grid and each housing layer. The RPA housing consists of a six-wafer stack of fusion bonded silicon wafers. Our RPA has grid apertures as small as 100µm. The springs are approximately 1cm long and capable of deflecting 200µm.

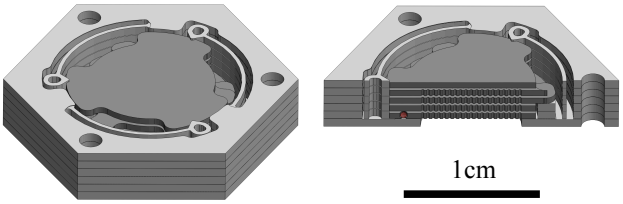

Figure 2: MEMS RPA schematic with cross-section.

Our design addresses the shortcomings of previous RPAs intended to measure plasmas with small Debye lengths. First, through the use of thick electrodes with high-aspect-ratio apertures, our micromachined RPAs remove the need for two successive ion-retarding grids; an added benefit of stiffer electrodes is the ability to bring these into closer proximity without risking deflection-induced shorting. The perimeter of each electrode contains contact tabs and alignment notches; these are etched simultaneously, ensuring self-alignment across the electrode stack.

Second, our RPA has a set of microfabricated deflection springs for robust and compliant alignment of the grid apertures across the grid stack, which greatly increases the signal strength and minimizes the ion interception. Improving upon in-plane assembly methods reported by Gassend et al. [11], our MEMS RPA extends our previous work [10] by replacing the alumina guide rails and a stainless steel housing with nitride-coated silicon springs. The physical dimensions of our RPA are thus reduced while further refining the sensor's assembly precision by approximately an order of magnitude (conventional machining tolerances are on the order of tens of microns, while Gassend et al. demonstrated accuracies of a few microns [11]). By using a curved geometry for the springs, the overall device footprint is further reduced.

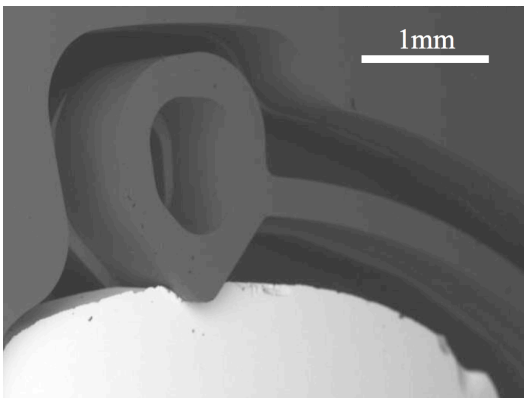

Figure 3: A MEMS deflection spring clamping a grid.

When assembled, each spring locks into the reference notches on the electrodes (Figure 3). By this dual function of gripping and aligning, the device becomes resistant to shifting and strains induced by thermal expansion. An added benefit from such modularity is the ability to use otherwise incompatible processing techniques in machining grids versus housing.

FABRICATION

The MEMS RPA consists of two major components, i.e., the housing and the electrodes. The housing of the RPA is created from a stack of six silicon wafers that are fusion bonded together; each wafer has a set of three curved deflection springs that include recesses to allow the individual actuation of each spring. The housing is fabricated using contact lithography, reactive ion etching (RIE), and deep reactive ion etching (DRIE) as main processing technologies. The housing is coated with a thermally grown silicon dioxide film that provides electrical insulation between the structure and the electrodes, and with a conformal layer of silicon-rich silicon nitride that acts as electrical insulator and prevents scratching the housing during electrode assembly. A 6-inch wafer stack yields 30 RPA housings. An exploded view of the MEMS RPA housing and a picture of a completed housing is shown in Figure 4.

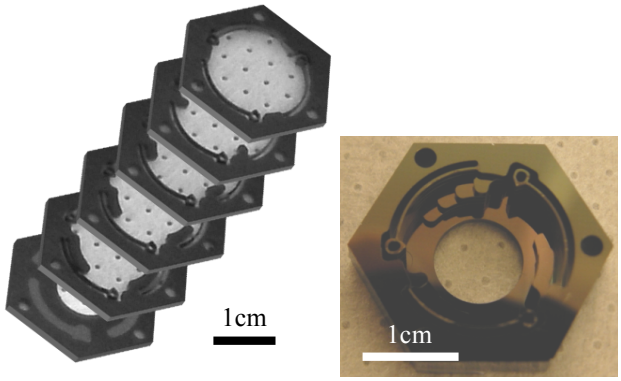

Figure 4: (left) exploded view of the six layers that compose the MEMS RPA housing; (right) completed housing.

The electrodes of the MEMS RPA are either perforated, i.e., grids, or solid, i.e., collectors. The process flow to fabricate the electrodes uses contact lithography, RIE, and DRIE as main processing technologies. The process flow was reported in [10]; however, the electrodes of our fully microfabricated sensors are coated with sputtered gold instead of sputtered tungsten. Integrating the grids and collector to the housing using the deflection springs completes the fabrication of the RPAs.

CHARACTERIZATION

Experimental characterization of our MEMS RPA was performed in a vacuum chamber equipped with an Ardara Technologies (Ardara, PA) Slim-Line^{TM} ionizer. A filament generates -50eV thermionic electrons that bombard the analyte, in this case air, at a pressure of around 3.5×10^{-5}Torr, ionizing the gas. In these experiments, the floating grid of the RPA was removed.

We first characterized three different RPAs under the same conditions to allow for a direct comparison of their performance. In these experiments, we tested a conventional RPA, a hybrid RPA, i.e., an RPA with microfabricated grids and housing machined using standard techniques [10], and our MEMS RPA. The results of these experiments are shown in Figure 5.

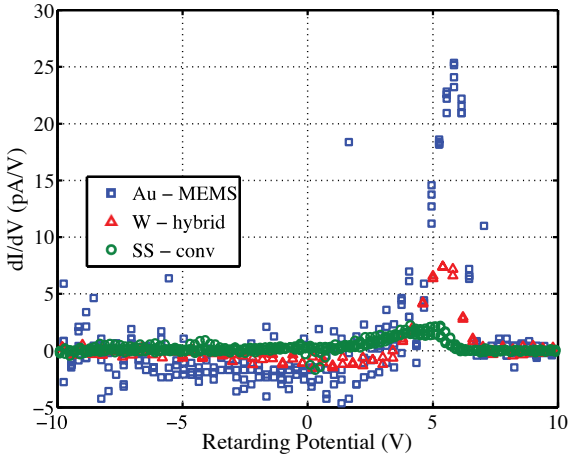

Figure 5: Ion energy distribution of an ion beam using our MEMS RPA, our previously reported hybrid RPA [10] and a conventional RPA. A tenfold increase in signal strength is apparent when compared against the conventional RPA.

In Figure 5, a threefold increase in the signal from the hybrid RPA compared to the signal from the standard RPA was observed; however, the increase does not correlate to the effective optical transparency of each RPA. On the one hand, the conventional RPA grids are made from perforated steel sheet with a hole-to-pitch ratio of 152:280, resulting in a grid transparency of 26.7%; if the three successive grids in the conventional RPA are assumed to be randomly oriented, an estimated effective optical transparency of only 1.9% is obtained. On the other hand, the tungsten-coated silicon grids of the hybrid RPA have 100µm diameter apertures at a 150µm pitch, resulting in a grid transparency of 40.3%; as a consequence of the mechanical alignment the electrodes in the hybrid design, the transparency can be assumed to be close to 40%. As Chao and Su, and Enloe and Shell suggested, the internal dynamics in an RPA are more complex than a simple matter of transparency [12],[13].

The ion energy distribution from the hybrid RPA shown in Figure 5 includes a non-physical negative distribution in the low-energy tail. We suspected that, as a consequence of the retarding potential and structured geometry, the changing field lines bring the flux of ions in and out of focus onto the collector plate as the voltage is swept; such a phenomena would explain why more ions seem to reach the collector as the bias is first increased toward and beyond 0V. Therefore, simulations were carried out using the Charged Particle Optics software (CPO Ltd., www.electronoptics.com) and verified that the electrode stack of the hybrid RPA had a collective lens effect. In addition to focusing, the ray traces of flowing ions at times intersected with the electrodes (namely the ion-retarding and secondary electron-repelling grids). We confirmed experimentally that in the hybrid RPA, a portion of the current transmitted by the ion-repelling grid was intercepted by the secondary electron-repelling grid (Figure 6).

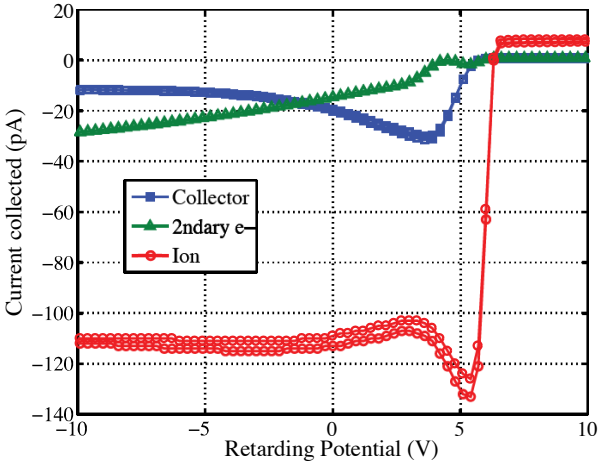

Figure 6: Collector current, secondary electron grid current, and ion-retarding grid current vs ion-retarding voltage showing ion interception by both electrodes.

Based on these observations, we improved the design of the electrode stack in our MEMS RPA. By using different aperture dimensions, as in Einzel lenses, ion interception can be minimized, and the non-physical negative component of the distribution is mitigated. We incorporated grids of 150µm, 250µm and 300µm aperture sizes with the same 400µm pitch into our sensor, effectively multiplexing the signal of numerous Einzel lenses onto one collector. With this arrangement, the MEMS RPA reported a threefold increase in peak signal over the hybrid version, or a tenfold improvement when compared to the conventional design (Figure 5). The transparency of the finest MEMS RPA grid is 12.8%, and we expect the effective transparency of the grid stack to be very similar to this value given the precise mechanical alignment enforced on the electrodes; this suggests that the signal strength in an RPA is not as much related on the effective optical transmission as on the capability of the electrode stack to minimize ion interception. Nonetheless, the estimated ion energy distribution we obtain from the MEMS RPA still has a low-energy negative tail, although it falls under the noise floor.

We further investigated the dependence of the signal-to-noise ratio (SNR) of the sensor on the effective optical transparency. Figure 7 shows the ion energy distribution estimated by MEMS RPAs with 150µm and 100µm grid apertures and the same aperture pitch. The transparency of the grids with 100µm apertures is 5.7%, i.e., a decrease by a factor of 2.25 compared to the transparency of the grids with 150µm apertures; although the peak amplitude is reduced by a proportional amount, the noise floor diminishes drastically for an improved SNR. We verified that for a MEMS RPA with grid stack with 100µm, 250µm, and 350µm grid apertures (for the electron repelling, ion retarding, and secondary electron repelling grids, respectively), the spurious low-energy tail almost completely vanishes.

We also verified the capability of our sensor to accurately follow changes in ion energy. In Figure 8, the

ion energy distribution was estimated as the ion energy of the source was progressively increased in two-volt increments. The MEMS RPA, as with our previous RPAs, closely tracks the change in ion energy; there is a constant 3-4eV offset between the estimated peak of the distribution and the nominal ion energy of the source. An increase in peak height with increasing energy is believed to point to limitations of the testing apparatus.

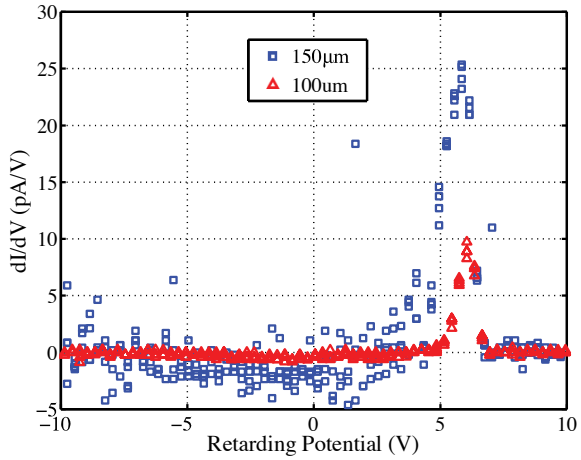

Figure 7: Ion energy distribution vs. ion-repelling grid voltage from MEMS RPAs with 100µm and 150µm grid apertures.

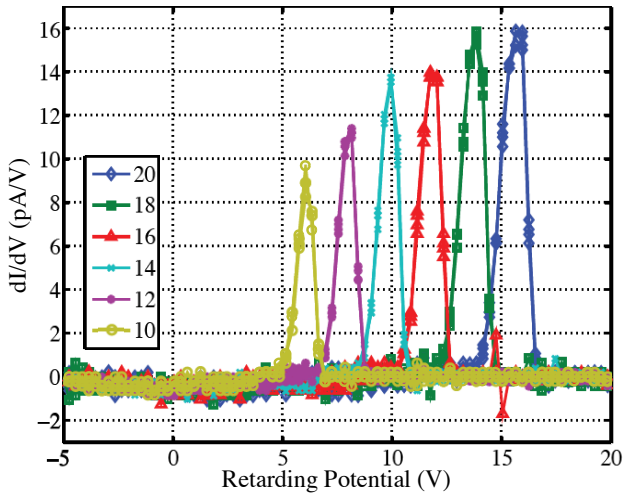

Figure 8: Ion energy distribution vs. ion repelling voltage for various ionization energies.

ACKNOWLEDGEMENTS

The authors express their gratitude to A. I. Akinwande (EECS, MIT) for providing access to the apparatus where the characterization of the devices was conducted. The devices were fabricated at the MIT's Microsystems Technology Laboratories. This work was supported in part by the United States National Aeronautics and Space Administration under contract No. NNC08CA58C (program managers T. Wallet and R. Manning), and by the United States Defense Advance Research Projects Agency Microsystems Technology Office under contract W31P4Q-11-1-0007 (program manager J. Judy). Any opinions, findings, and conclusions or recommendations expressed in this publication are those of the authors and do not necessarily reflect the views of the US Government and therefore, no official endorsement of the US Government should be inferred.

REFERENCES

[1] L. B. King, "Transport-Property and Mass Spectral Measurements in the Plasma Exhaust Plume of a Hall-Effect Space Propulsion System," Ph.D. dissertation, Univ. of Michigan, 1998.

[2] Y. Azziz, "Experimental and Theoretical Characterization of a Hall Thruster Plume," Ph.D. dissertation, Massachusetts Inst. of Technology, Cambridge, MA, 2007.

[3] B. E. Beal and A. D. Gallimore, "Energy analysis of a Hall thruster cluster," *Tech. Dig. 28th Int. Electric Propulsion Conf.*, Toulouse, France, 2003.

[4] R. R. Hofer, J. M. Haas, and A. D. Gallimore, "Ion voltage diagnostics in the far-field plume of a high-specific impulse Hall thruster," *Tech. Dig. 39th Joint Propulsion Conf.,* Huntsville, AL, 2003.

[5] K. M. Lemmer, A. D. Gallimore, T. B. Smith, and D. R. Austin, "Review of two retarding potential analyzers for use in high density helicon plasma," *Tech. Dig. 30th Int. Electric Propulsion Conf.*, Florence, Italy, 2007.

[6] J. M. Partridge, "Development and Implementation of Diagnostics for Unsteady Small-Scale Plasma Plumes," Ph.D. dissertation, Worcester Polytechnic Inst., 2008.

[7] I. H. Hutchinson, *Principles of Plasma Diagnostics*, Cambridge University Press, New York, NY, 2nd ed., 2002.

[8] C. M. Marrese, N. Majumdar, J. M. Haas, G. Williams, L. B. King, and A. D. Gallimore, "Development of a Single-orifice Retarding Potential Analyzer for Hall Thruster Plume Characterization," *Tech. Dig. 25th Int. Electric Propulsion Conf.*, pp. 397-404, 1997.

[9] J. M. Partridge, "Development of a Micro-Retarding Potential Analyzer for High-Density Flowing Plasmas," M.S. thesis, Worcester Polytechnic Inst., 2005.

[10] E. V. Heubel, A. I. Akinwande, and L. F. Velásquez-García, "MEMS-Enabled Retarding Potential Analyzers for Hypersonic In-Flight Plasma Diagnostics," *Tech. Dig. Solid-State Sensor, Actuators and Microsystems Workshop*, Hilton Head, SC, pp. 324-327, 2012.

[11] B. Gassend, L. F. Velásquez-García, and A. I. Akinwande, "Precision In-Plane Hand Assembly of Bulk-Microfabricated Components for High Voltage MEMS Arrays Applications," *J. Microelectromech. Syst.*, vol. 18, pp. 332-346, 2009.

[12] C. K. Chao and S.-Y. Su, "Charged particle motion inside the retarding potential analyzer," *Physics of Plasmas*, vol. 7, pp. 101-107, 2000.

[13] C. L. Enloe and J. R. Shell, "Optimizing the energy resolution of planar retarding potential analyzers," *Review of Scientific Instruments*, vol. 63, pp. 1788-1791, 1992.

CONTACT

*E. V. Heubel, tel: +1-617-253-0728; evheubel@mit.edu